

AD-A229601



# Measurements of Acoustic Reflection From the End of a Cylindrical Block of Arctic Ice

by  
G. R. Garrison  
R. E. Francois  
T. Wen  
R. P. Stein

Accession For	
NTIS CRA&I	<input checked="" type="checkbox"/>
DTIC TAB	<input type="checkbox"/>
Unannounced	<input type="checkbox"/>
Justification	
By	
Distribution /	
Availability Codes	
Dist	Avail and/or Special
A-1	

**APL-UW 8506  
September 1986**

**Applied Physics Laboratory University of Washington  
Seattle, Washington 98105**

*Approved for Public Release; Distribution is Unlimited*

**Contract N00024-81-C-6042  
Contract N00024-85-C-6264**

### ACKNOWLEDGMENTS

*This work was performed for the NAVSEA Arctic USW Environmental Technology Program, NAVSEA 63R, Mr. D.E. Porter, under PE62759N, Subproject SF59-555. This subproject was block managed by Mr. R.L. Martin, NORDA Code 113. The authors appreciate the helpful discussions with Dr. S.R. Murphy and Dr. E.I. Thorsos of APL-UW.*

## CONTENTS

	<i>Page</i>
I. INTRODUCTION.....	1
II. EXPERIMENTAL ARRANGEMENT.....	3
III. THEORETICAL TREATMENTS.....	7
A. Impedance Change.....	7
B. Rigid Plate Reflections.....	8
C. Combined Effects.....	8
D. Near-Field Effects.....	9
E. Sound Absorption in Ice.....	12
IV. MEASUREMENTS.....	13
A. Data Summary.....	13
B. Two Echoes in the Return.....	13
C. Returns at Normal Incidence.....	16
D. Aspect Dependence.....	19
V. SUMMARY.....	32
VI. DISCUSSION.....	33
REFERENCES.....	35

## LIST OF FIGURES

	<i>Page</i>
Figure 1. Arrangement for the ice block experiment .....	3
Figure 2. The framework for controlling the transducer from the surface.....	4
Figure 3. (a) Closeup of the notched frame and pegged beam used to position the transducer, which was supported by three lines 120° apart.....	5
(b) The framework placed near the block.....	5
(c) The framework placed near the block.....	6
(d) Transducer assembly being lowered through the diver access hole.....	6
Figure 4. Interference patterns predicted for reflection from a rigid, circular plate combined with the loss (9.5 dB) due to the impedance change .....	9
Figure 5. Computed target strength with corrections for near-field effects at a range of 15 m .....	11
Figure 6. Return from the ice block on Run 6 at 80 kHz, N20-E16, 0.5 ms cw pulse.....	14
Figure 7. Spacing of the ice block for the experiments on 3-5 November 1984.....	15
Figure 8. Comparison of first echo, second echo, and overlapping of the two in the return at 80 kHz on Run 6 .....	15
Figure 9. Upper surface reflection coefficients calculated for Run 6 at 80 kHz along with calculated relative phase of the two reflections.....	18
Figure 10. Response patterns for a 0.84 m diam. ice block.....	19
Figure 11. A test of the empirical equation, $TS = A - B\theta$ .....	26
Figure 12. Measured target strengths at normal incidence.....	30
Figure 13. The constant B in Eq. 8 as determined from the measurements listed in Table VII.....	31

## LIST OF TABLES

	<i>Page</i>
Table I. Acoustic properties of ice and water.....	7
Table II. Phase difference at edge of face.....	10
Table III. Near-field effect.....	10
Table IV. Absorption of sound in ice for temperatures between -20°C and -2°C as calculated using the equation $\alpha = 0.06 f (-6/T)^{2/3}$ dB/m.....	12
Table V. Measurements of reflections from an ice block.....	14
Table VI. The echo amplitudes used to calculate target strength, and the amplitude reflection coefficients $R_A$ computed for the lower face, for all runs.....	17
Table VII. Constants for the line $TS = A - B \theta$ .....	29

### ABSTRACT

In the fall of 1984 an experiment was conducted at an arctic ice camp to examine 20-80 kHz acoustic reflections from an isolated ice block. The results are compared with a simple model of ice block reflections that has been used in conjunction with an ice block configuration for pressure ridge keels. The study of the reflections from these keels is important because they form an interfering background for acoustic equipment operating under the ice. A cylindrical block of ice 0.84 m in diameter was cut from the flat surface of a floe and depressed so that, for a transducer placed below, the reflection from the block would arrive before that from the surrounding ice. A transducer 15-30 m below the block was moved horizontally in steps to measure changes with aspect. The returns from the block are compared with those predicted by the model, which includes a loss based on the bulk impedance properties of the two media. When near field effects are included, the measured returns at 20 kHz are similar to those predicted; but as the frequency is increased the return at normal incidence is lower than predicted and the response pattern is broadened and smoothed. The complex structure of the growing sea ice, producing both volume and surface acoustic scattering, is the most likely cause of the discrepancy.

## I. INTRODUCTION

In the arctic the ice canopy is stressed by the wind, causing differential movements which form pressure ridges and keels of all shapes and sizes. These keels are a disruptive influence on the transmission of sound beneath the ice and thus have a large effect on the performance of acoustic equipment in this medium.

Measurements of ice-keel reflections in 1982 revealed that they come from individual, point-like reflectors which tend to appear and disappear with small changes in aspect, giving a sporadic distribution for reflections along the keel.<sup>1</sup> Possible configurations that could produce such reflections include blocks with a face toward the source, blocks forming a corner reflector, and blocks that are tilted so as to reflect to the surface and back to the receiver.

In the fall of 1984, an experiment was devised to examine one of these configurations, a block of ice with a face at near-normal incidence. For this experiment, a cylindrical block was cut from a flat section of a floe and depressed so that, for a transducer placed below, the reflection from the block's face would arrive before the reflection from the under surface of the floe and thus be distinguishable. As the echo amplitudes were recorded, the transducer was moved successively along a line to change the aspect.

The immediate purpose of this report is to compare the measured falloff of target strength at incident angles near normal with a theoretical approximation presently used for ice keel modeling.<sup>2</sup> This theory uses the Kirchhoff approximation to combine the change in impedance at the water-ice interface and the interference pattern for reflection from a circular plate. Near-field effects are also computed.

The results show that at 20 kHz the measured reflection is a few decibels lower than theory, but the response pattern is approximately as predicted. At higher frequencies the return at normal incidence is considerably lower than predicted, and the measured response pattern drops off with very little sign of the nulls and peaks that are present in the theoretical diffraction pattern. Apparently the surface and volume properties of the porous ice at and near the interface provide a transition layer that cannot be treated as a sharp water-ice boundary. The effect of the gradual transition is to weaken and smooth the response. Further investigation is needed on the surface and volume scattering properties of growing sea ice. The following summary of the freezing process may be helpful.

Sea ice is a very inhomogeneous material. Freezing starts at the sea surface with small disk-shaped particles (platelets) which grow horizontally in a snowflake-like pattern. As freezing continues and the platelets begin to crowd each other, they eventually tip to a vertical position. In the process, brine is concentrated between them. The freezing process continues with the downward growth of the ice platelets. Eventually the space between the platelets freezes, accompanied by displacement and some entrapment of the brine concentrate. The vertical platelets at the freezing interface form a "skeletal layer" which is quite fragile. The thickness of the skeletal layer depends on the temperature gradient in the ice; the temperature varies from about  $-1.8^{\circ}\text{C}$  at the lower surface to the air temperature at the upper surface. The entrapped brine remains in solution, in temperature equilibrium, down to about  $-23^{\circ}\text{C}$ . Below  $-23^{\circ}\text{C}$ , most of the brine is a solid precipitate. Above  $-23^{\circ}\text{C}$ , for a given bulk salinity, the brine volume depends on the temperature. Entrapped air and gases, displaced from seawater, also contribute to the porosity of ice and may be an important element in the acoustic response of sea ice. For the ice samples studied in this experiment, the close-off of pores due to temperature probably occurred 2 or 3 cm from the platelet tips, giving rise to an "equivalent acoustic roughness" of many millimeters.

The result of the experiment will be helpful in determining if a flat ice block face at normal incidence is a major source of the sporadic reflections from an ice keel. An identification of the ice configurations in a keel that cause acoustic reflections is essential for preparing models of the ice for acoustic studies.



## II. EXPERIMENTAL ARRANGEMENT

The experiment was conducted on an ice floe in the Beaufort Sea on 3-5 November 1984. The arrangement for the experiment is shown in Fig. 1. Polypropylene lines running through oil-filled pipes inserted through the ice supported the transducer from three directions  $120^\circ$  apart. These lines were tied to a ring above the surface, and the transducer was moved by moving the ring. The arrangement on the surface is shown in Fig. 2. A framework near the submerged ice block supported a beam on which pegs were spaced every 15 cm. All four sides of the frame were notched at 15 cm intervals so that the beam containing the pegs could be moved sideways or rotated perpendicularly. By moving the ring successively along the line of pegs above the ice, the transducer was moved along a corresponding line below the ice with an exaggeration that was easily calculable. The calculation was facilitated by orienting the framework so that its centerline extended through one of the pipes holding the lines.

Installation began with divers examining the under side of the floe and selecting a relatively flat area. A 4 in. (10 cm) diam. hole was drilled 0.3 m deep in the 0.46 m thick ice at the selected location. A 2 in. (5 cm) diam. aluminum pole was installed as vertically as possible in the hole, and fresh water was poured in to help freeze the pole in place. The next day, a 0.84 m diam., circular block was cut out around the pole, pushed

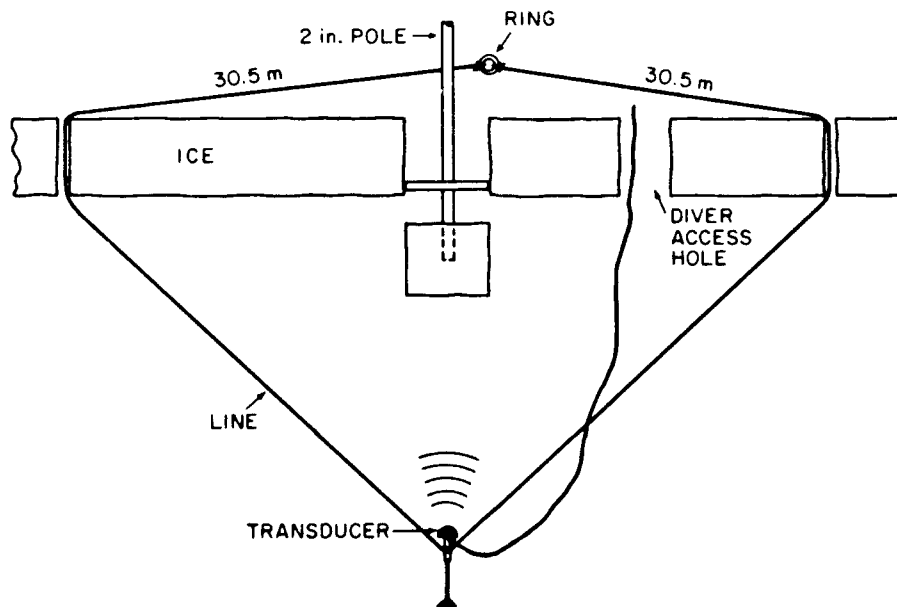


Figure 1. Arrangement for the ice block experiment.

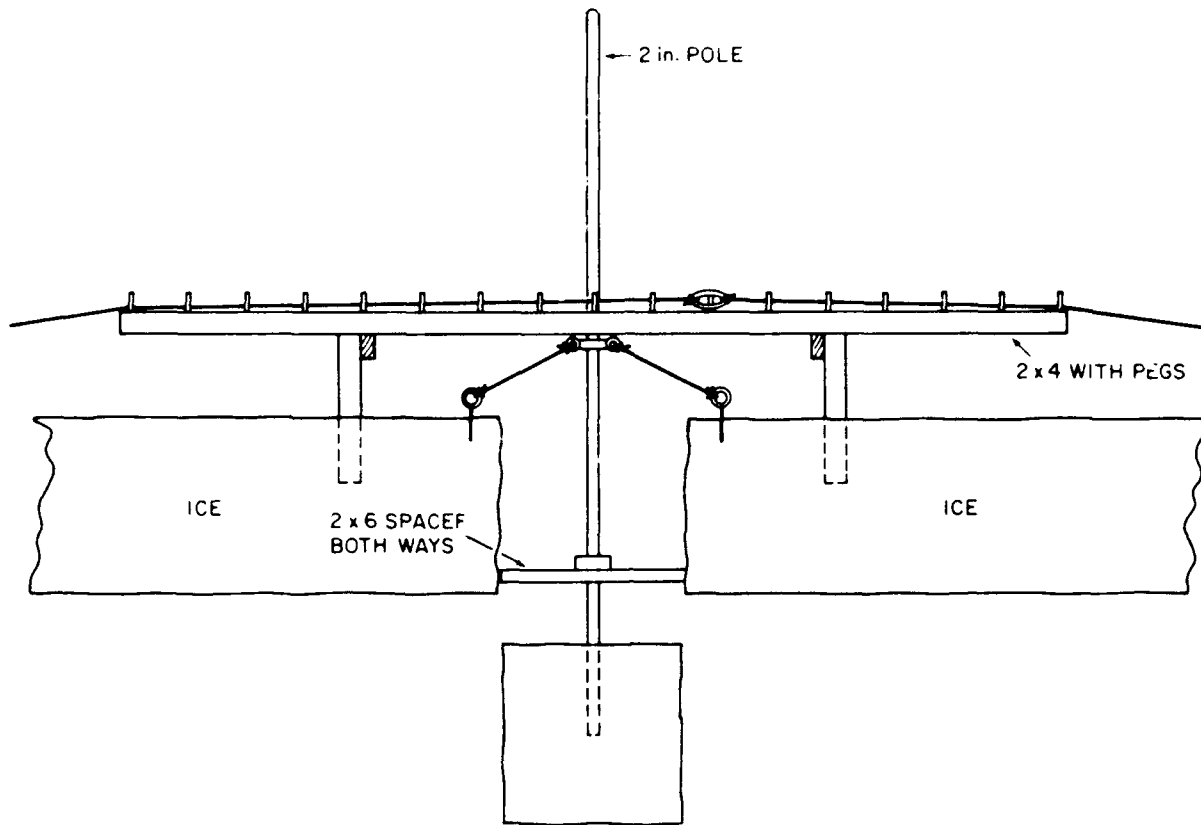
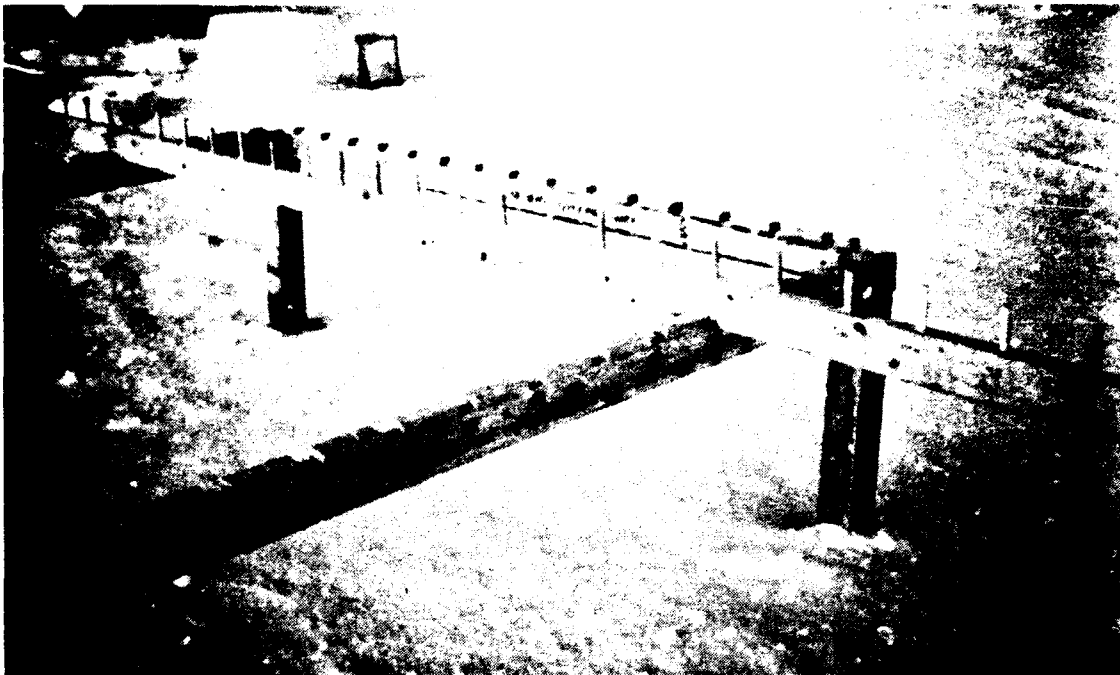


Figure 2. The framework for controlling the transducer from the surface.

downward 0.6 m, and guyed into position. A circular block was used so that its orientation with respect to the frame did not need to be determined. The divers then helped install the lines for the transducer. Once the lines were available at the surface, the transducer was connected and lowered to the desired depth.

Photographs of the arrangement as installed in the field are shown in Fig. 3. Fuel oil was poured into each of the three plastic pipes through which the lines were threaded to keep them free. The electronics cable from the transducer extended 100 m to a heated building which housed the instrumentation. Communication between the field crew and the instrument room was by radio.



*Figure 3(a). Closeup of the notched frame and pegged beam used to position the transducer, which was supported by three lines 120° apart.*



*Figure 3(b). The framework placed near the block. A 2-in. (5-cm) diam. aluminum tube was installed vertically in the ice before cutting out the block.*



*Figure 3(c).*

*The framework placed near the block. A metal ring, placed over one of the pegs, held the ends of the three lines at the desired location.*



*Figure 3(d).*

*Transducer assembly being lowered through the diver access hole. A lead weight kept the transducer vertical.*

### III. THEORETICAL TREATMENTS

The reflection of plane waves from an ice block face has been predicted by Ellison<sup>2</sup> based on a combination of two separate phenomena which are incorporated in the Kirchhoff approximation.<sup>3</sup> One is the reflection loss due to the change in acoustic impedance at the water-ice boundary. The other is the interference pattern produced in the reflected wave by individual contributions from separate elements of the finite block face. In addition, we consider near-field effects and refer to ice absorption measurements.

#### A. Impedance Change

For a plane wave impinging on an infinite surface, the amplitude of the reflection,  $A_r$ , is related<sup>4</sup> to the amplitude of the incident plane wave,  $A_i$ , by the amplitude reflection coefficient

$$R_A = \frac{A_r}{A_i} = \left[ \frac{\rho_i c_i}{\rho c} - B \right] \left[ \frac{\rho_i c_i}{\rho c} + B \right]^{-1}. \quad (1)$$

When applied to the water-ice interface  $\rho_i$  and  $c_i$  are the density and sound speed for ice, and  $\rho$  and  $c$  are the density and sound speed for water;

$$B = \sqrt{1 + \left[ 1 - \frac{c_i^2}{c^2} \right] \tan^2 \theta_i},$$

where  $\theta_i$  is the incident angle. For normal incidence,  $B = 1$ .

The values used for these properties are shown in Table I. The values for water were measured in the field,<sup>5</sup> whereas those for ice were estimated from measurements reported by others<sup>6</sup> for arctic ice.

Table I. Acoustic properties of ice and water.

Ice	Water
$\rho_i = 0.92 \text{ g/cm}^3$	$\rho = 1.022 \text{ g/cm}^3$
$c_i = 3200 \text{ m/s}$	$c = 1433 \text{ m/s}$
Impedance Ratio = $\frac{\rho_i c_i}{\rho c} = \frac{2944}{1465} = 2.01$	

Inserting these values in Eq. 1, we obtain for normal incidence ( $B=1$ )

$$R_A = \frac{A_r}{A_i} = 0.34, \quad (2)$$

which represents a decrease in intensity of 9.5 dB for the reflected sound. The shear wave should also be considered, but its effect is very small for angles of  $0^\circ$ - $15^\circ$ , the range of angles encountered in the experiment.

### B. Rigid Plate Reflections

If we consider the block face as a fixed, rigid plate (following the Ellison approach), the theoretical target strength of a return at incident angle  $\theta$  is given by<sup>7</sup>

$$TS = 20 \log \left[ \left[ \frac{\pi a^2}{\lambda} \right] \left[ \frac{2J_1(\beta)}{\beta} \right] \cos \beta \right] \text{ (dB)}, \quad (3)$$

where

$$\begin{aligned} \beta &= \frac{(4\pi a)}{\lambda} \sin\theta \\ \lambda &= \text{wavelength} \\ k &= 2\pi/\lambda \\ a &= \text{radius of plate.} \end{aligned}$$

For this equation to be valid, there should be no appreciable near-field effects (i.e.,  $R \gg a^2/\lambda$ , where  $R$  = range) and the Kirchhoff approximation for a flat plate must be valid (i.e.,  $ka \gg 1$ ). For our measurements, the minimum range was 14.5 m and the maximum  $a^2/\lambda$  was 9.8, indicating some near-field effect. Our minimum  $ka$  was 37, well above 1.

### C. Combined Effects

If we combine the effects of the impedance change and the finite plane pattern, we obtain the following equation for the target strength of the block face:

$$TS = 20 \log \left[ R_A \frac{\pi a^2}{\lambda} \frac{2J_1(\beta)}{\beta} \cos\theta \right], \quad (4)$$

where  $R_A = (Q-1)/(Q+1)$ ;  $Q$  is the ratio of the impedance of the ice to that of the water; i.e.,

$$Q = \frac{\rho_i c_i}{\rho c}$$

Equation 4 predicts that the return will drop rapidly as the angle departs from normal incidence, but in addition there are interference peaks and valleys whose spacing depends on the frequency. Figure 4 shows, as examples, the returns at three frequencies from a circular plate of radius 0.42 m as computed from Eq. 4.

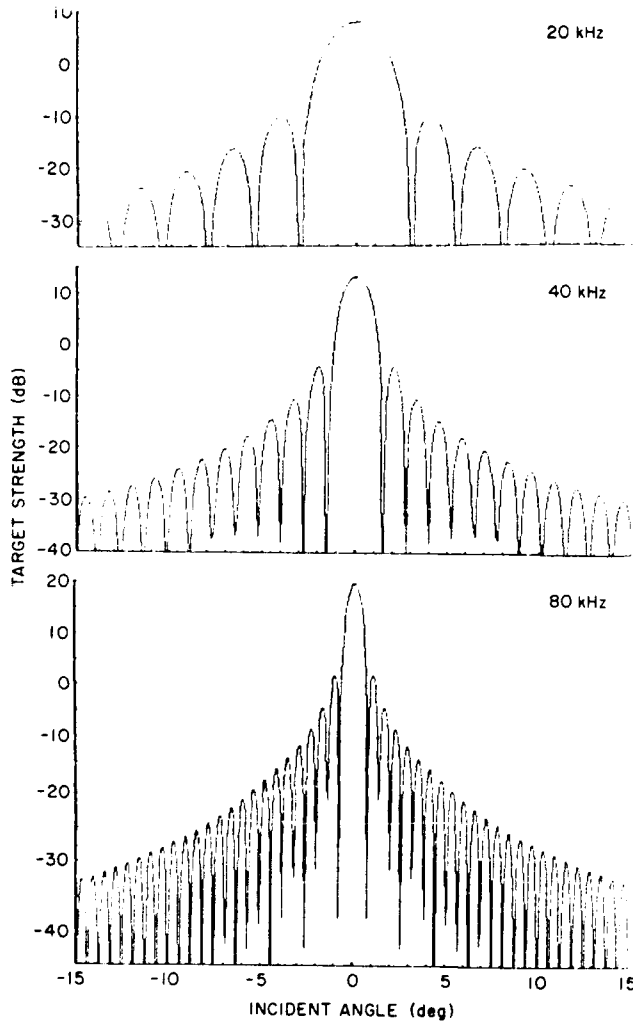


Figure 4.

*Interference patterns predicted for reflection from a rigid, circular plate combined with the loss (9.5 dB) due to the impedance change.*

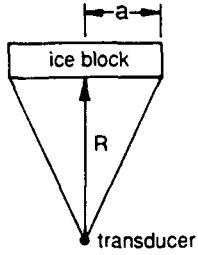
#### D. Near-Field Effects

For short ranges, the possibility of near-field effects should be investigated. The possibility can be assessed by comparing the phase of contributions from the edge of the block face with that of those from the center, at normal incidence. The phase difference  $P$  is calculated by

$$P = 2 \left[ \sqrt{R^2 + a^2} - R \right] \frac{2\pi}{\lambda} \quad (\text{radians}), \quad (5)$$

where  $a$  is the radius of the face. Table II shows the phase differences calculated for the frequencies and ranges used in the experiment. For the shorter range, the phase shift is considerable at 40 kHz and higher.

Table II. Phase difference at edge of face.

Frequency (kHz)	Phase Difference (deg)		(radius $a = 0.42$ m)
	$R = 14.5$ m	$R = 32.9$ m	
20	61	27	
40	122	54	
47	143	63	
80	244	107	

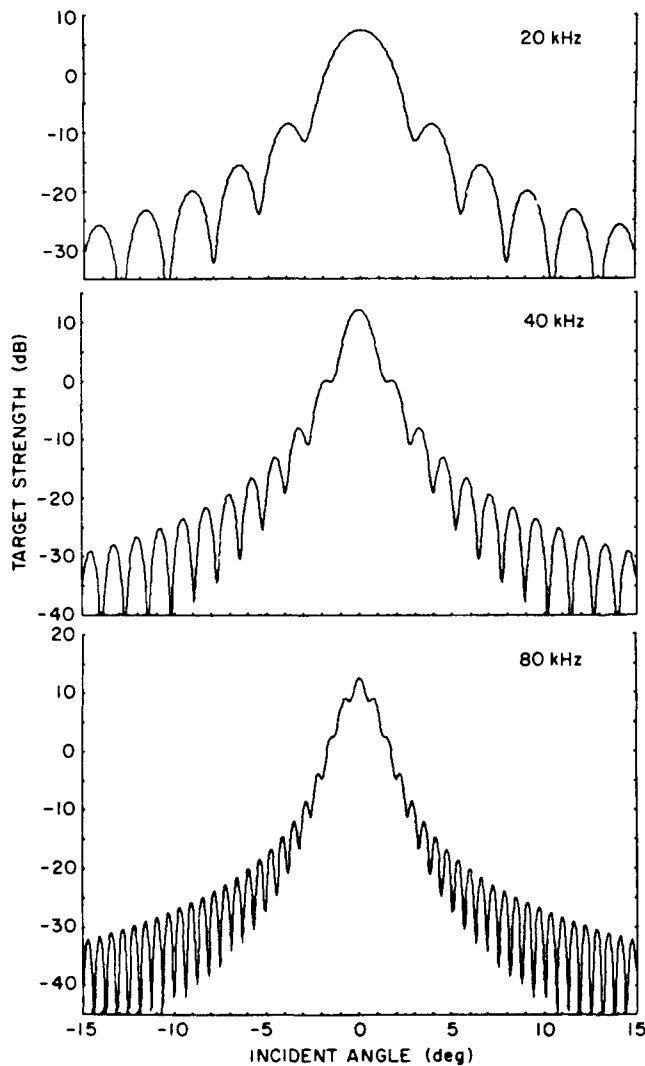
To determine the effect of the phase differences, we numerically integrate outward over concentric, circular rings, adding the in-phase component of each area. The sum divided by the area is designated  $f$ . Calculated values of  $f$  are given in Table III along with the calculated reduction in target strength,  $-20 \log f$ . Table III shows that the short-range measurements require an appreciable near-field correction.

Table III. Near-field effect.

Frequency (kHz)	Area Factor $f$		Target Strength Reduction (dB)	
	$R = 14.5$ m	$R = 32.9$ m	(Runs 5-7) $R = 14.5$ m	(Runs 1-3) $R = 32.9$ m
20	0.95	0.99	0.4	0.1
40	0.83	0.96	1.6	0.3
47	0.77	0.95	2.3	0.4
80	0.41	0.86	7.7	1.3



The angular dependence can be computed by numerically integrating over ring segments. The results for the shortest range used in the experiment, 15 m, are shown in Fig. 5. The main lobe is reduced, and the nulls at the smaller angles tend to be bridged across.



*Figure 5.*  
*Computed target strength with corrections for near-field effects at a range of 15 m. Compare with Figure 4.*

### E. Sound Absorption in Ice

The simple model proposed by Ellison does not account for any contribution to the observed target strength from volume scattering or from rear surface reflection. In our analysis, we investigated a second reflection, apparently from the upper surface of the block, which was originally an air-ice interface. Evaluating the returns from the upper face of the block requires knowledge of the absorption coefficient in the ice. With no theory available, we used a recent summary of absorption measurements by McCammon and McDaniel<sup>6</sup> which indicates that the absorption of compressional sound waves of frequency  $f$  (kHz) in ice of temperature  $T$  (°C) is

$$\alpha = 0.06f (-6/T)^{2/3} \quad (\text{dB/m}) \quad (6)$$

for  $T$  limited to  $-2^\circ$  to  $-20^\circ\text{C}$ .

The air temperature was about  $-20^\circ\text{C}$  during the days prior to cutting the block.<sup>5</sup> The water temperature was  $-1.5^\circ\text{C}$ . After the block was submerged for 4 days, its average temperature was somewhere between the initial average of  $-11^\circ\text{C}$  ( $-20^\circ$  at the top and  $-1.5^\circ\text{C}$  at the bottom) and the water temperature of  $-1.5^\circ\text{C}$ . Table IV shows the absorption for the temperatures and frequencies of interest as calculated using Eq. 6.

Table IV. Absorption of sound in ice<sup>6</sup> (decibels/meter) for temperatures between  $-20^\circ\text{C}$  and  $-2^\circ\text{C}$ , as calculated using the equation  $\alpha = 0.06f (-6/T)^{2/3}$  dB/m.

T (°C)	Frequency (kHz)			
	20	40	47	80
$-1.5^a$	3.0	6.1	7.1	12.1
-5	1.4	2.7	3.2	5.4
-10	0.9	1.7	2.0	3.4
-15	0.7	1.3	1.5	2.6
-20	0.5	1.1	1.3	2.2

<sup>a</sup>Extrapolated slightly beyond limit of equation.

NOTE: The two-way path through the ice block was 0.92 m.

#### IV. MEASUREMENTS

To position the transducer relative to the ice block, a gridwork was established on the surface with position 0,0 in the southwest corner. The positions, which were at 15 cm intervals, were labeled according to their distance north or east of this point. Each coordinate had 32 positions. A wooden beam with vertical pegs spaced every 15 cm was oriented north-south or east-west in a square framework notched at 15 cm intervals. In this way, any line of peg positions could be provided. A set of measurements labeled line N20, for example, would be obtained with the beam oriented east-west in the 20th position north of 0,0. The ring connected to the lines holding the transducer would then be moved along the line from one peg to another.

For the experiment, short pulses were transmitted at either 20, 40, 47, or 80 kHz and received on the same transducer. The returns were observed for about 10 s on a Nicolet digital oscilloscope, and the average amplitude of the reflections was estimated. After several trials to locate the position producing the maximum return, the ring was moved from peg to peg along two perpendicular lines intersecting that position, and the average amplitude at each location was recorded by hand. In addition, one set of returns at 80 kHz was digitized on the oscilloscope, and the results were recorded on a diskette. This made possible later examination of the echo in detail.

The center of the framework was at grid position N16-E16, but this was not necessarily the location that placed the transducer directly beneath the block. On the first day the center of the block appeared to be at N18-E18. After the lines were shortened for the measurements on the second day, the center was near N20-E18.

##### A. Data Summary

The first three "runs" were made on 3 November with the transducer at a depth of 33.9 m. At that depth, the transducer moved horizontally 41% more than the ring. On 5 November the lines were shortened, raising the transducer to a depth of 15.5 m, and three more runs were made. At this depth, the transducer moved only about 10% more than the ring, and the returns were stronger. The runs are summarized in Table V. The pulse length was 1.0 ms for Runs 1 and 2, and 0.5 ms for the remaining runs.

##### B. Two Echoes in the Return

The envelopes of the returns on Run 6, which used an 80 kHz, 0.5-ms-long cw pulse, were digitized on the Nicolet oscilloscope, preserved on diskette, and examined later in detail. A sample return is shown in Fig. 6. Note the two overlapping echoes. The second echo arrived only 0.3 ms after the first and well before the echo from the under side of the adjacent floe, the start of which is shown at the right in the figure. The

Table V. Measurements of reflections from an ice block.

Run No.	Date	Transducer Depth <sup>a</sup> (m)	Frequency (kHz)	Transmitter Voltage <sup>b</sup> (V)	Total Gain (dB)	Type of Transducer	Receiving Sensitivity (dB) <sup>c</sup>	Transmitting Response (dB) <sup>d</sup>
1	3 Nov 84	33.9	47	200	79	2" piston	-195	156
2			47	200	79		-195	156
3	5 Nov 84		80	620	80	ITC 1042	-207	150
5		15.5	40	660	82		-208	136
6			80	530	82		-207	150
7			20	520	94		-207	123

<sup>a</sup>The lower face of the block was at a depth of 1 m.

<sup>b</sup>Peak-to-peak

<sup>c</sup>Decibels are referenced to 1 V/ $\mu$ Pa.

<sup>d</sup>Decibels are referenced to 1  $\mu$ Pa/V at 1 m.

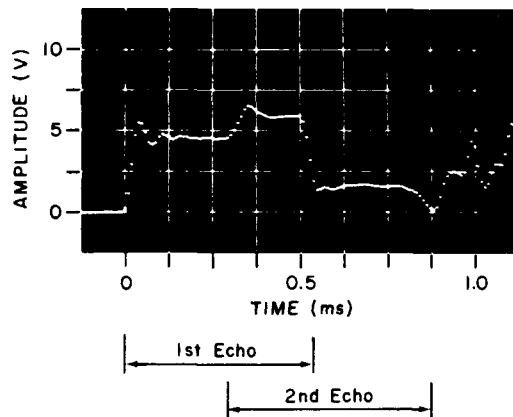


Figure 6.

Return from the ice block on Run 6 at 80 kHz, N20-E16, 0.5 ms cw pulse.

dimensions of the arrangement (Fig. 7) and the expected sound speed in the ice enable us to calculate that the first echo is from the lower face of the block, the second echo is from the upper face, and the following echoes are from the adjacent ice. Figure 8 compares the levels of the first, second, and overlapping returns for line N20 of Run 6. The overlap should represent the vector sum of the echoes from the top and bottom faces of the block. The amplitude of the overlap was near the algebraic sum for the two echoes, indicating that the amplitudes added coherently for the particular thickness of the ice block used in the experiment. The phase difference would include a 180° change at the upper face.

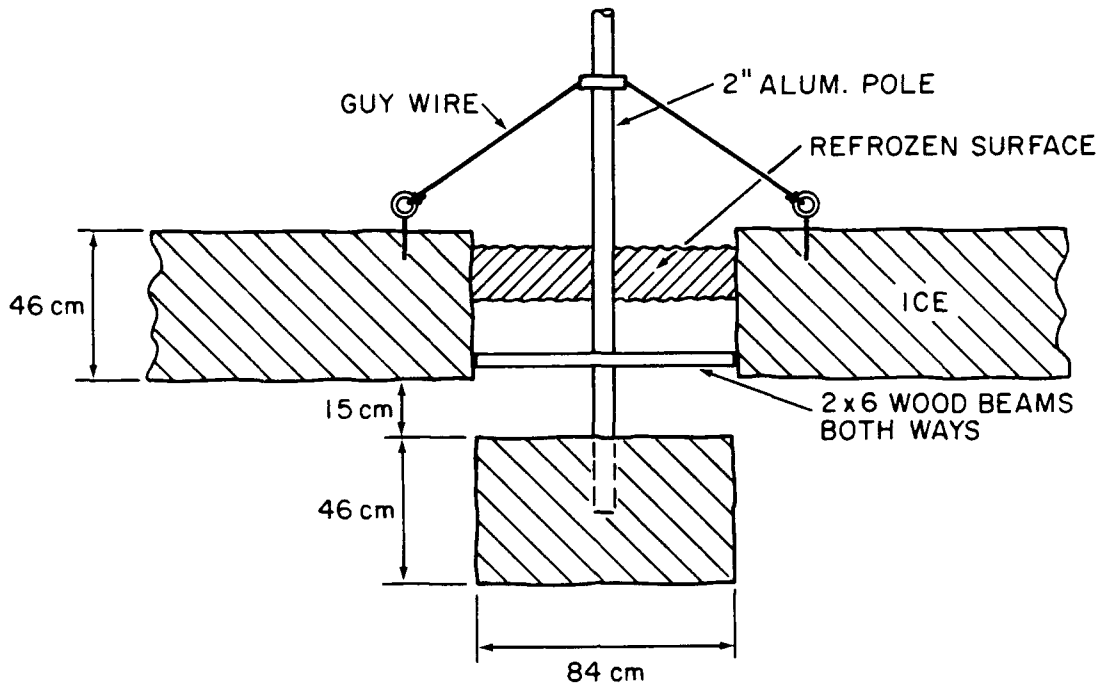


Figure 7. Spacing of the ice block for the experiments on 3-5 November 1984.

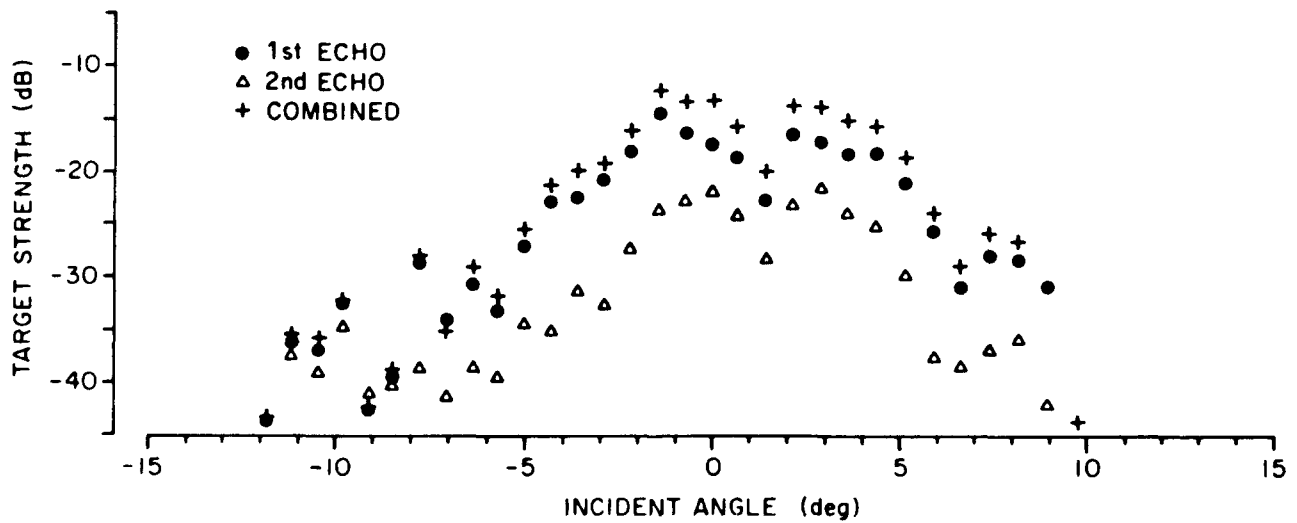


Figure 8. Comparison of first echo, second echo, and overlapping of the two in the return at 80 kHz on Run 6; line N20.

The presence of echoes from the upper face at the other frequencies is uncertain. Two sample oscillograms of the returns on Run 2, which used a 47 kHz, 1 ms long pulse, were saved, and they show a gradual rise in amplitude rather than distinct levels. Because of experiment time constraints, no oscillograms were saved of the measurements at 20 and 40 kHz, which used a 0.5 ms pulse. Furthermore, an additional reflection from the upper face of the ice block was not readily apparent in any of the echoes examined in detail during the experiment. Readings of maximum signal level were made in real time and logged manually; consequently, the measurements could represent the maximum of the first, second, or overlapping echo. For the detailed observations at 80 kHz, which did show two echoes, the difference between the amplitude of the first echo and the maximum amplitude was small (Fig. 8). The smaller absorption at the lower frequencies would tend to enlarge the returns from the upper surface, but with no multiple levels observed we are uncertain as to the effect of the second surface on our readings.

### C. Returns at Normal Incidence

The 80 kHz echoes were examined in the returns at incident angles near zero. The amplitudes of returns at these angles, which were assumed to represent the lower face, are tabulated in Table VI along with the target strength calculated from the transducer calibrations and the two-way transmission losses. Also shown are the reflection coefficients,  $R_A$ , computed by solving for  $R_A$  in Eq. 4 and making the near-field correction given in Table III.

Equation 2 predicts an  $R_A$  of 0.34 for the density and sound speed values involved in the experiment. The value shown in Table VI for 20 kHz (0.24) is a little below 0.34, while the values shown for the other frequencies are far below, indicating that Eq. 4 is unacceptable at these frequencies. An additional correction involving the scattering processes at the lower surface is apparently needed, the more so the smaller the wavelength.

As mentioned earlier, the reflection measurements on Run 6 at 80 kHz gave the amplitude of the return from the upper face. The reflection coefficient for the upper face can be computed by comparing the reflections from the upper and lower surfaces, if some rather bold assumptions are made. We assume that the reflection coefficient at the lower face is given by the impedance ratio (Eq. 2,  $R_A = 0.34$ ) and that both returns are affected the same by the shape of the ice face. Reflection from the lower face changes the amplitude of the incident sound by the factor  $R_A$ . For sound entering the ice, the amplitude is changed by  $1+R_A$ ; at the reflection off the upper face it is changed by an unknown factor,  $R_B$ , and as it passes through the lower face it is changed by  $1-R_A$ . In addition, the sound suffers absorption losses both ways through the ice. These changes are shown in the following equation for the difference in the two returns:

$$(TS)_B - (TS)_A = 20 \log(1+R_A) + 20 \log(1-R_A) + 20 \log R_B - 20 \log R_A - 2 \alpha t, \quad (7)$$

Table VI. The echo amplitudes used to calculate target strength, and the amplitude reflection coefficients  $R_A$  computed for the lower face, for all runs.

Run	Frequency (kHz)	Transducer Position		Reflection Amplitude (V, peak)	Target Strength (dB)	Average	$R_A$ from Eq. 4
1	47	E18	N17	2.1	-12.0	-12.8	0.013
			N19	1.8	-13.6		
			N20	1.5	-14.9		
		N18	E17	2.0	-12.4		
			E18	2.3	-11.7		
			E19	2.1	-12.0		
2	47	E18	N19	1.7	-14.0	-15.1	0.010
			N20	1.6	-14.4		
			N21	1.6	-14.4		
		N20	E16	1.1	-17.7		
			E17	1.5	-14.9		
			E19	1.5	-15.4		
3	80	E18	N20	1.6	-6.9	-7.0	0.017
			N21	1.9	-5.4		
			N22	1.7	-6.4		
		N20	E14	1.3	-8.6		
			E15	1.6	-6.9		
			E16	1.5	-7.5		
5	40	E18	N19	2.3	-6.4	-6.0	0.039
			N20	2.4	-6.0		
			N21	1.7	-9.1		
		N20	E15	2.0	-7.7		
			E16	3.6	-2.5		
			E17	3.1	-4.0		
6	80	E18	N19	4.0	-14.4	-15.1	0.014
			N20	3.5	-15.4		
			N21	3.2	-16.5		
		N20	E16	4.5	-13.6		
			E17	3.7	-15.4		
			E18	3.6	-15.4		
7	20	E18	N19	6.4	4.30	4.84	0.237
			N20	7.1	5.25		
			N21	6.7	4.76		
		N20	E17	6.4	4.35		
			E18	7.1	5.25		
			E19	7.0	5.11		

where  $t$  is the thickness of the ice block. For a given  $R_A$  and  $\alpha$ , the equation can be solved for  $R_B$ , the reflection coefficient for the upper face.

The absorption in the ice varies with temperature as shown in Table IV. The temperature of the ice was initially  $-20^\circ\text{C}$  at the upper surface and  $-1.5^\circ\text{C}$  at the lower. Run 6 was made after the ice had been submerged for 2 days. The average temperature was somewhere between the initial average,  $-11^\circ\text{C}$ , and an ultimate equilibrium temperature of  $-1.5^\circ\text{C}$ . In calculating  $R_B$ , the reflection coefficient for the upper surface, we used both  $-6$  and  $-2^\circ\text{C}$  to show how the calculated  $R_B$  depends on the assumed temperature.

The results are plotted in Fig. 9 for two lines of Run 6, N20 and E18. The reflection coefficient depends strongly on the value used for the sound absorption in the ice, varying by a factor of 2 for the given variation in ice temperature. The coefficients for  $-6^\circ\text{C}$ , the more likely average temperature, are near the value (0.34) calculated for the impedance change from ice to water, indicating that the upper surface (originally snow covered) represents the same change in density and sound speed as the lower face.

When the reflections from the upper and lower surfaces overlap, the result appears to be a coherent addition of the two reflections with a phase difference of about  $45^\circ$  as shown in the upper graph of Fig. 9. The amplitude of the overlap is definitely greater than for an incoherent addition; coherence seems to prevail even after the sound has passed through the block and reflected from the upper surface.

At the other frequencies, the contribution from the upper face was not detected during the experiment, and no records are available for further analysis.

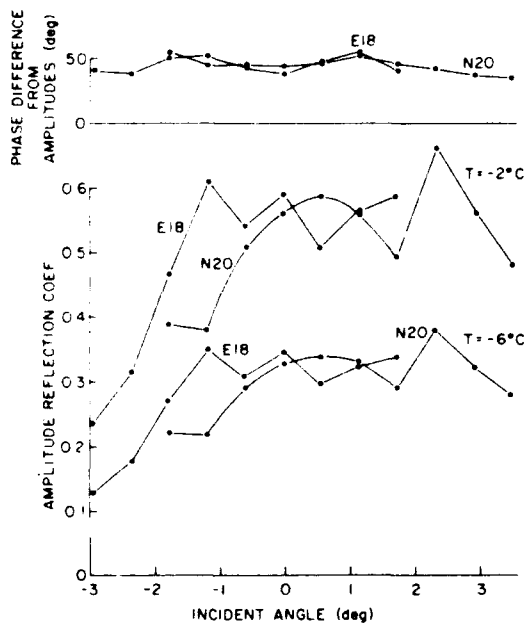


Figure 9.

Upper surface reflection coefficients calculated for Run 6 at 80 kHz (bottom) along with calculated relative phase of the two reflections (top).



### D. Aspect Dependence

To investigate the effect of changes in aspect angle, the transducer was moved successively along a line beneath the block. At each position, the location of the transducer and the aspect angle of the sound incident on the block's face were calculated from the geometry of the supporting lines. The amplitude of the return was then converted to target strength and plotted versus the calculated aspect angle. The results are shown in Fig. 10. The characters following the run number indicate the line along which the ring controlling the transducer's position was moved.

The data points in Fig. 10 are compared with the theoretical pattern predicted by Ellison,<sup>2</sup> who uses the Kirchhoff approximation in combining impedance change and rigid plate reflection. Near-field effects are included in the figure for the short range runs (5, 6, and 7). The high peak predicted near  $0^\circ$  was never observed, but the dropoff with angle beyond  $\pm 2^\circ$  is about as predicted. There is an occasional indication of the predicted side lobes, but the minima are spaced farther apart. Some lines did not pass directly below the ice block; for plots of these, the theoretical return was calculated for an offset from center. The predicted sharp minima were detected so rarely that at this time they will be ignored.

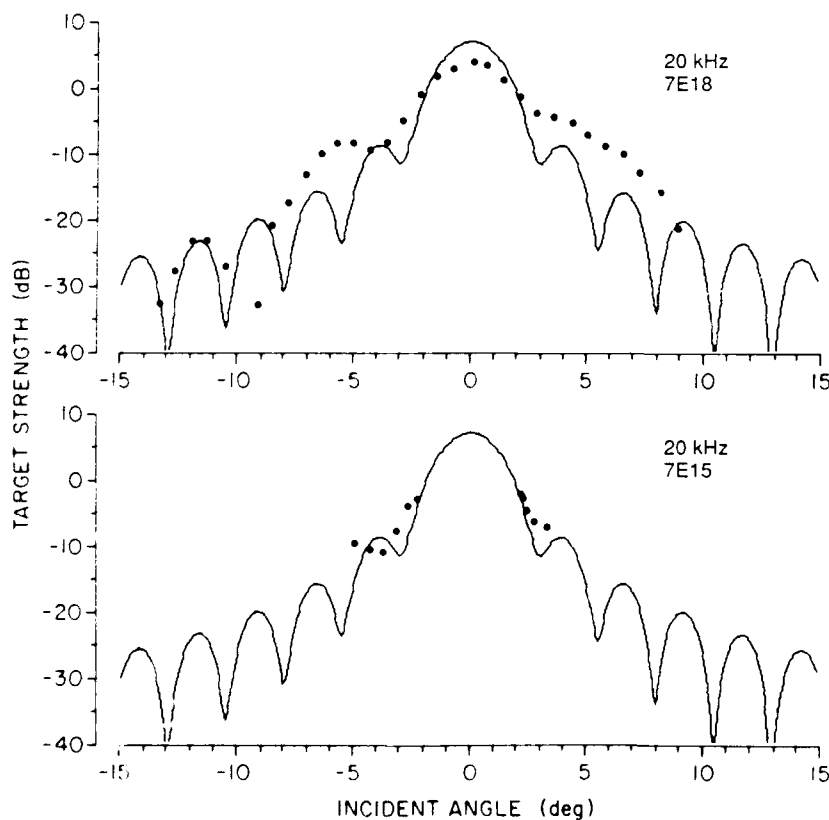


Figure 10.

Response patterns for a 0.84 m diam. ice block. The lines are the theoretical pattern for a rigid plate, combined with impedance change. Corrections for near field have been made for the short range measurements. (Continued on the following pages.)

Figure 10, cont.

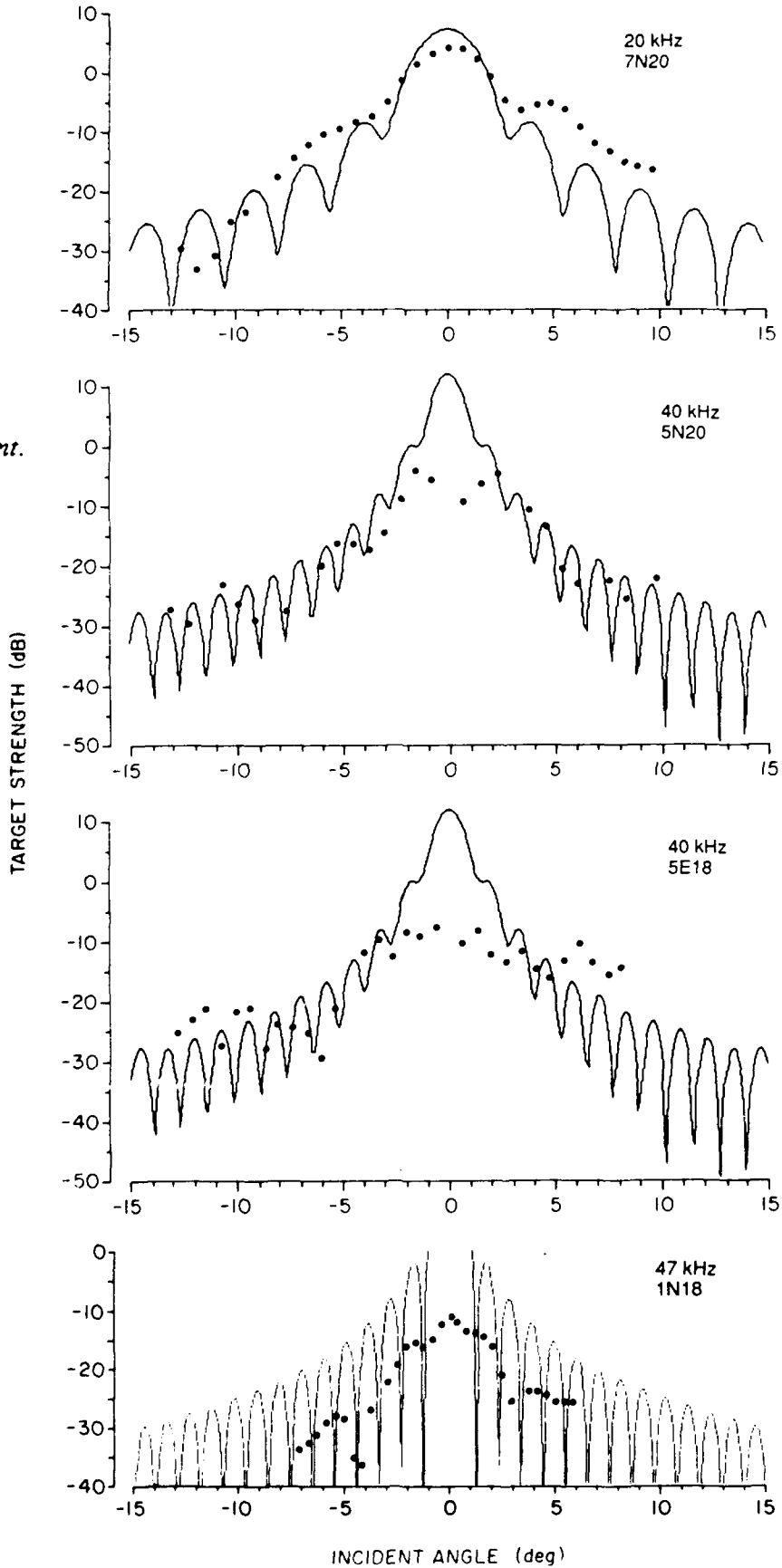


Figure 10, cont.

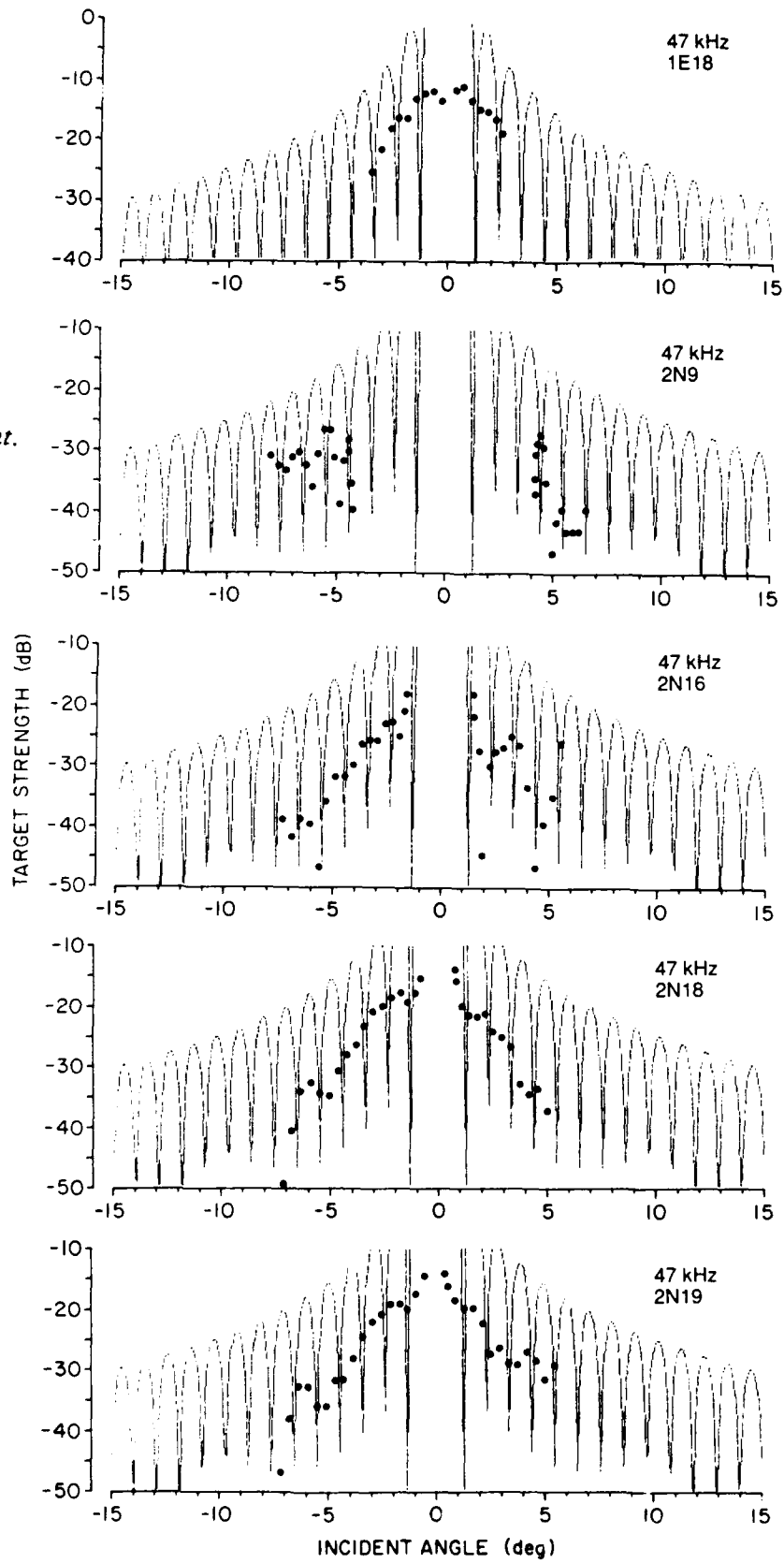


Figure 10, cont.

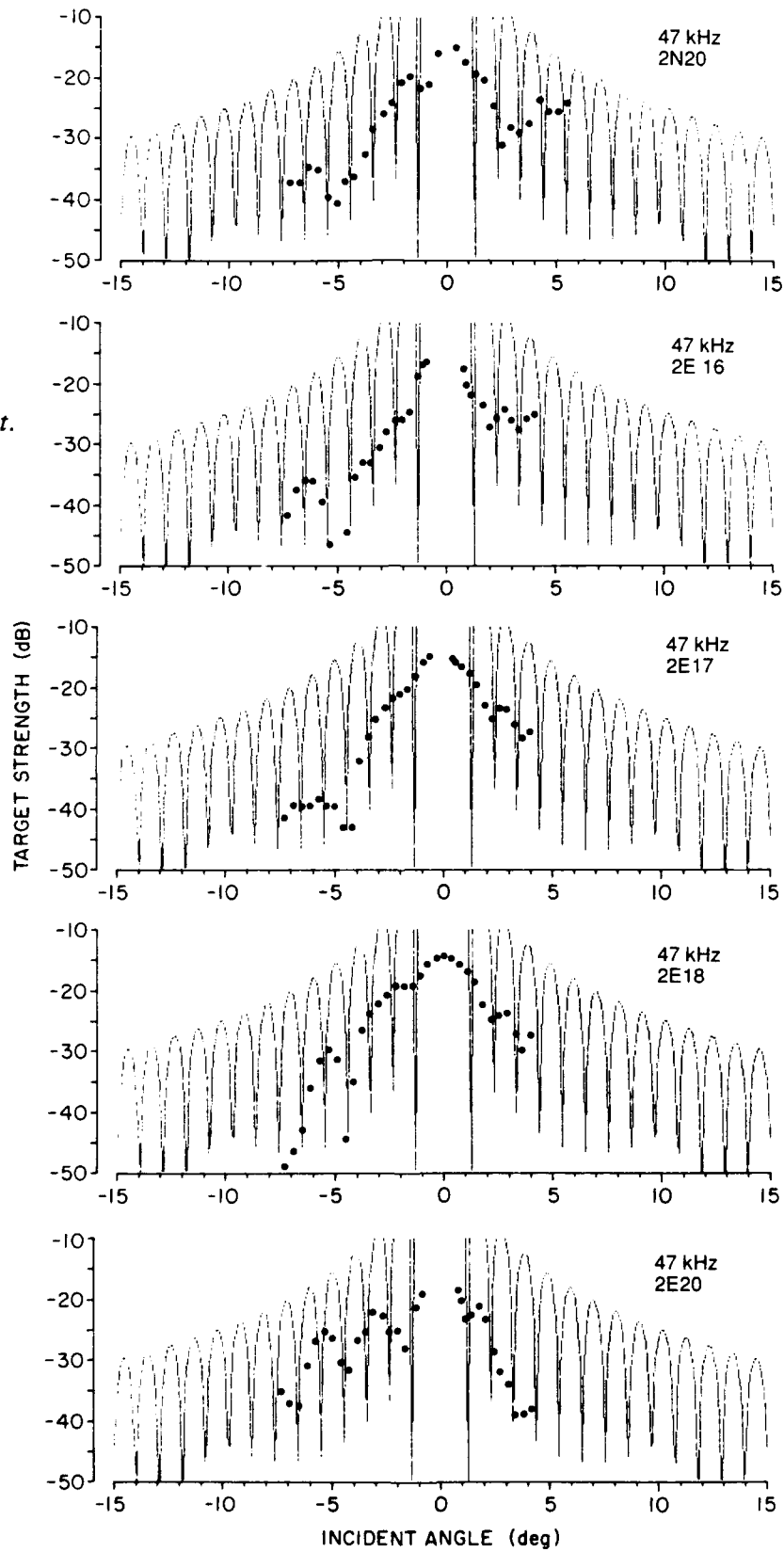


Figure 10, cont.

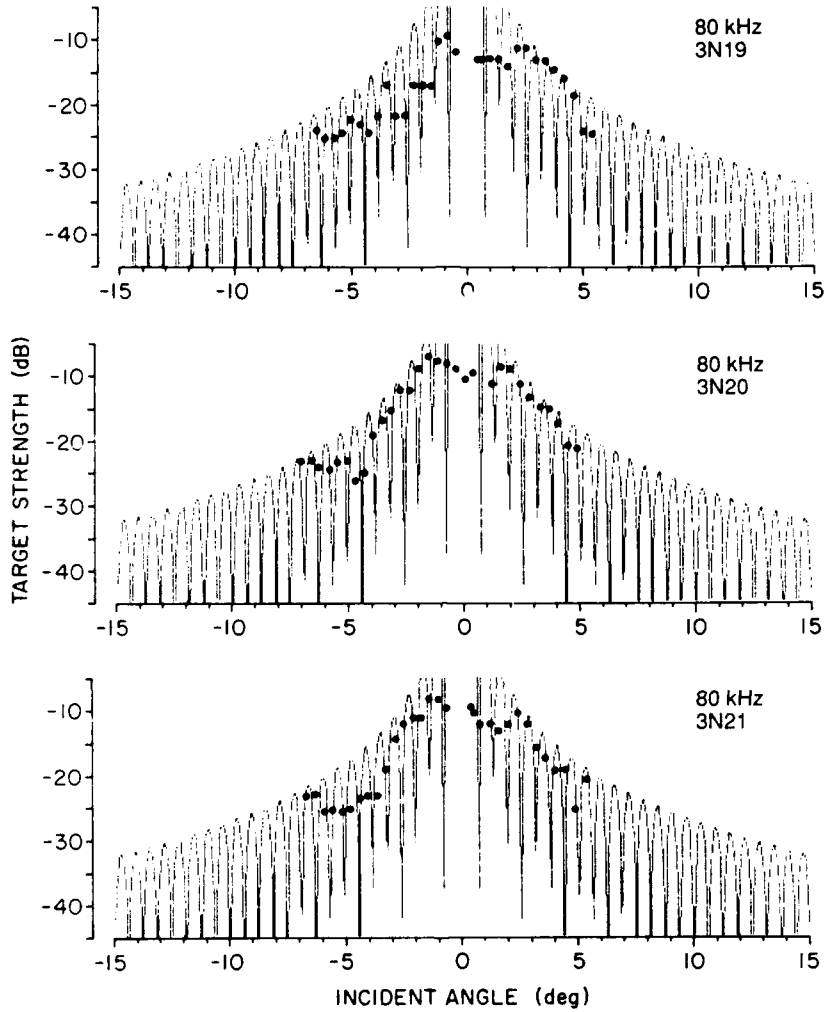


Figure 10, cont.

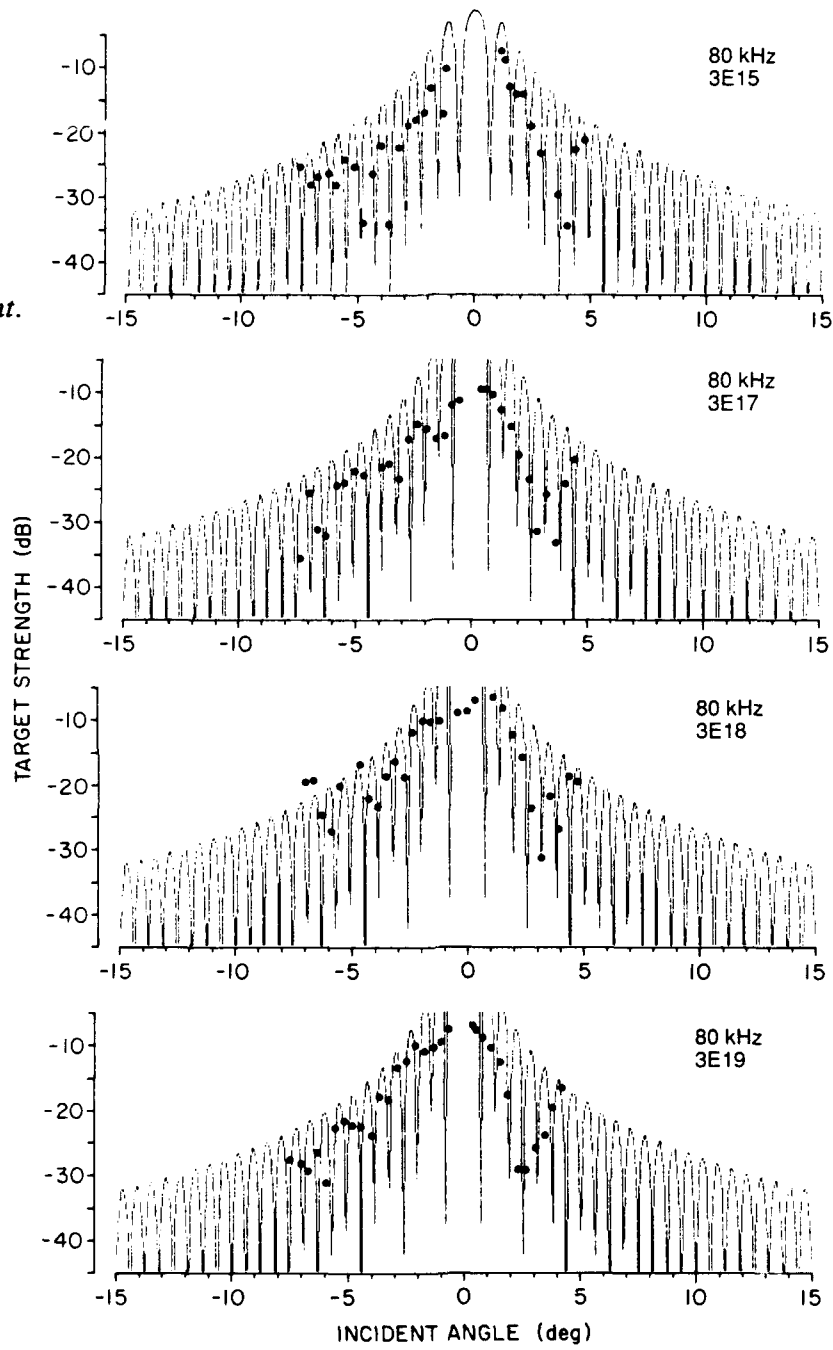
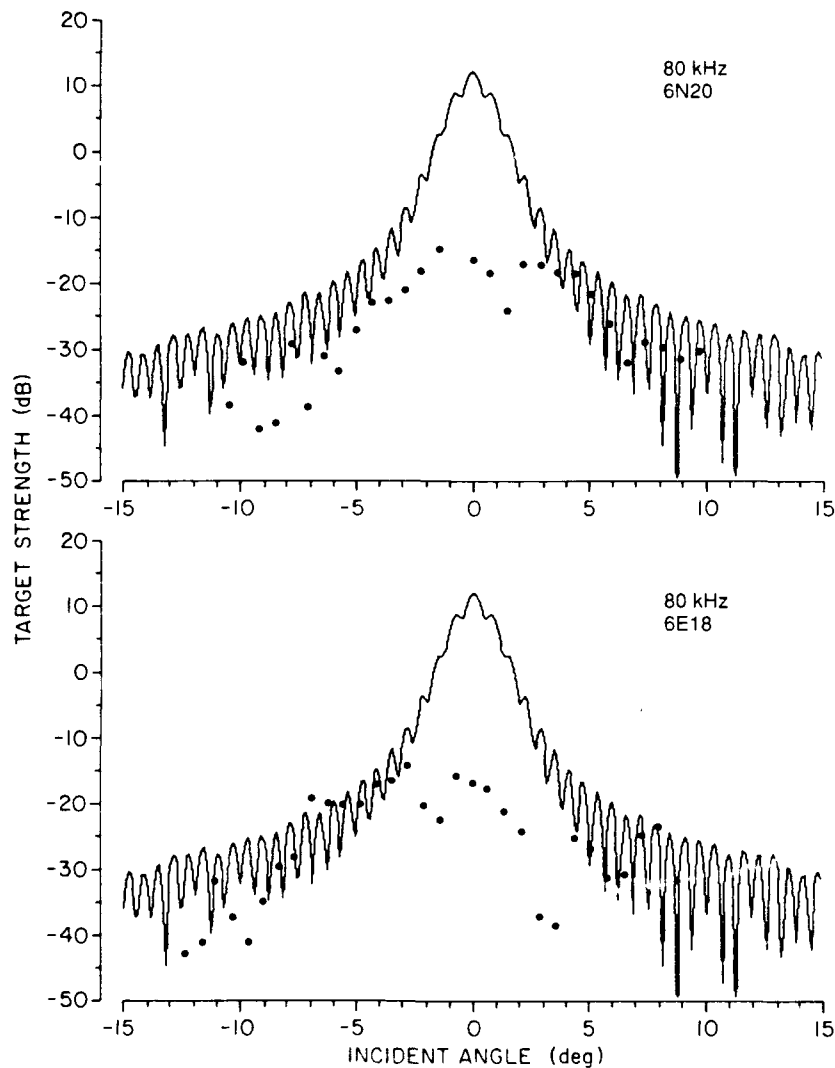


Figure 10, cont.



To test the form of the aspect dependence, the plots of target strength versus incident angle in Fig. 10 were folded over to combine plus and minus incident angles, and the data were fitted, using a least-squares method, by the line

$$TS = A - B\theta. \quad (8)$$

As shown in Figs. 11a-c, the lines appear to represent the data. Considering the scatter in the data, a more complex dependence on angle is not warranted.

The constants  $A$  and  $B$  for each line are listed in Table VII along with the average for each set. The averages for  $A$  have been adjusted for the near-field correction shown in Table III. Note that the 80 kHz data for the two transducer depths are brought into agreement by the near-field correction.

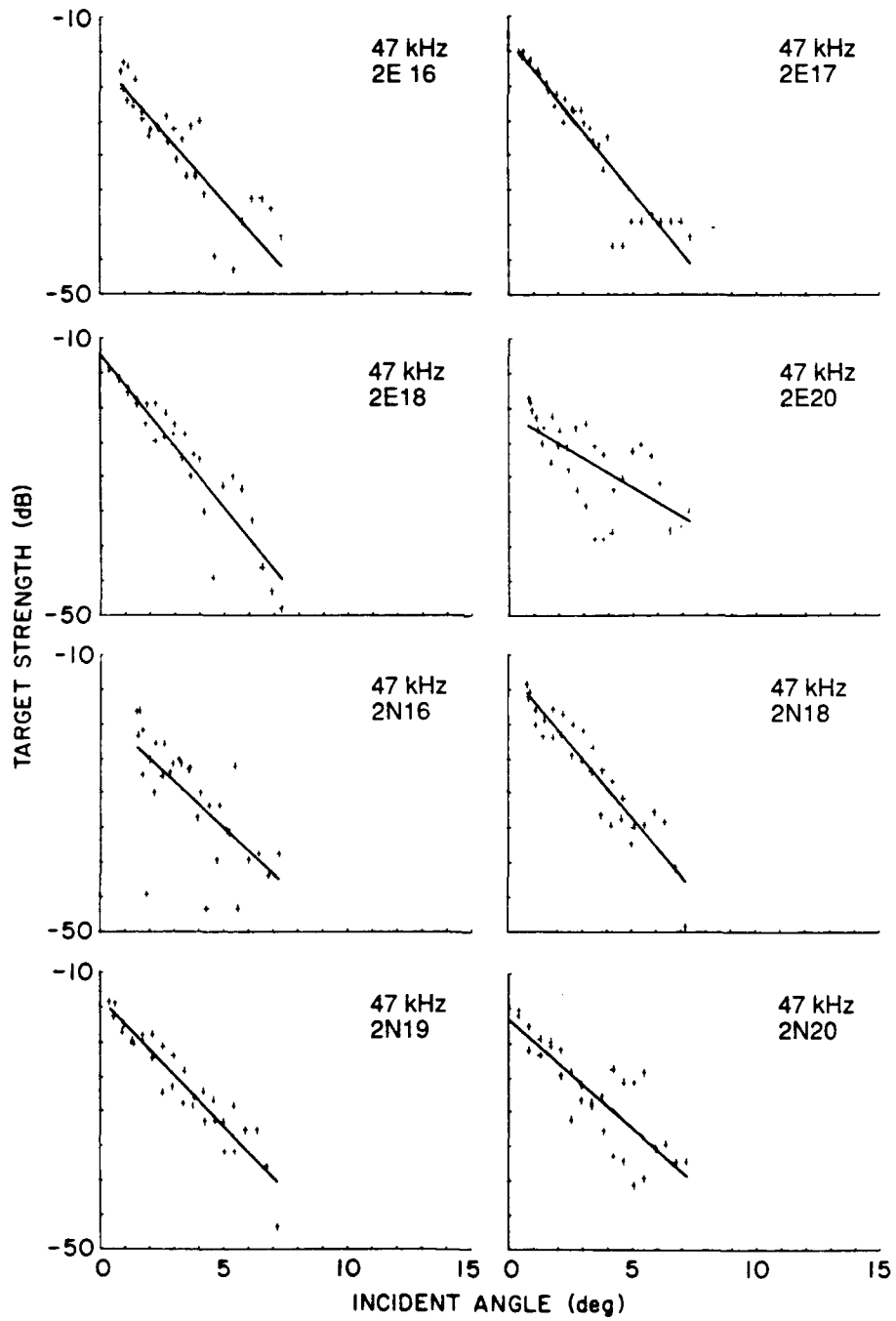


Figure 11a. A test of the empirical equation,  $TS = A - B\theta$ .



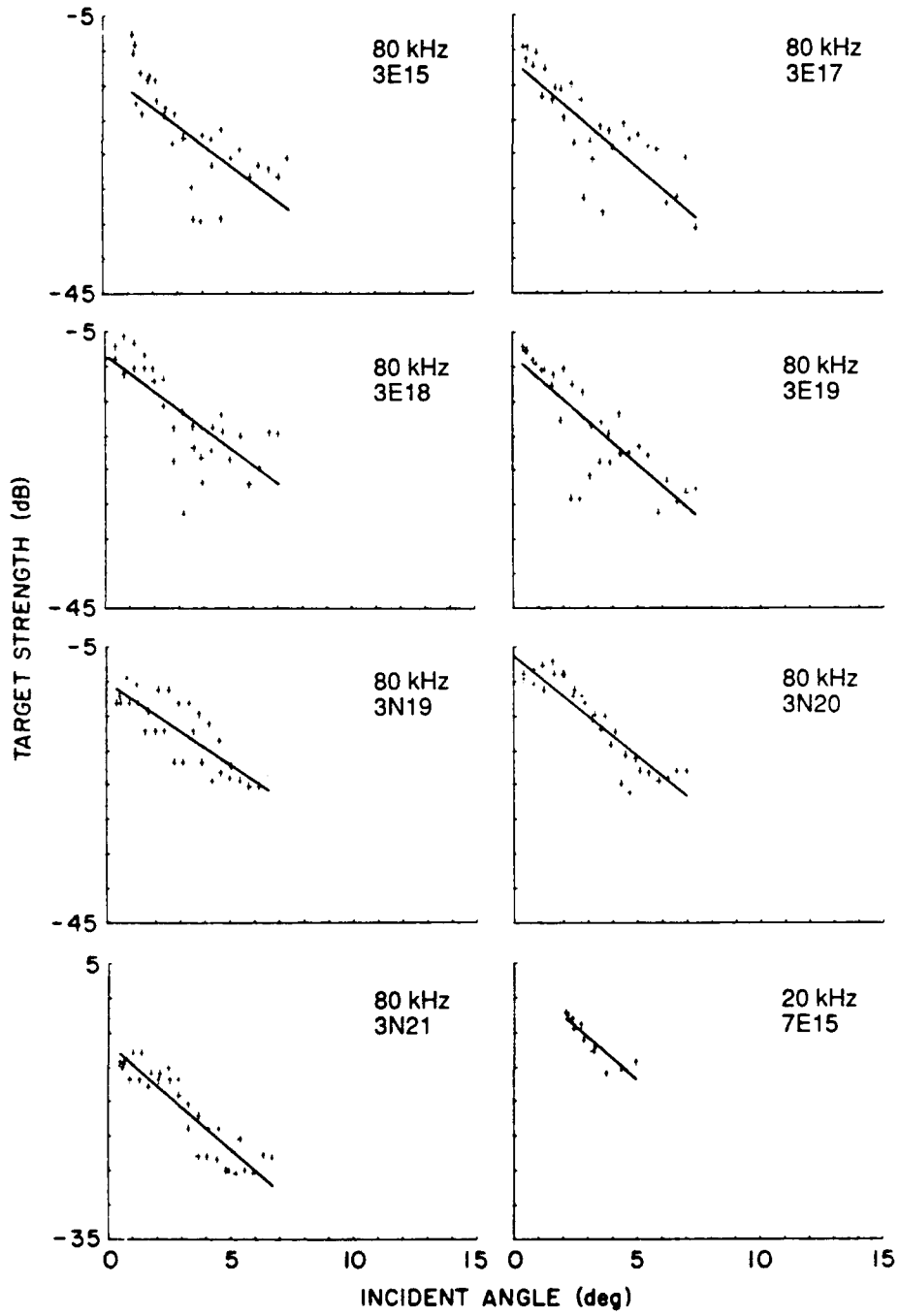


Figure 11b. A test of the empirical equation,  $TS = A - B\theta$ .

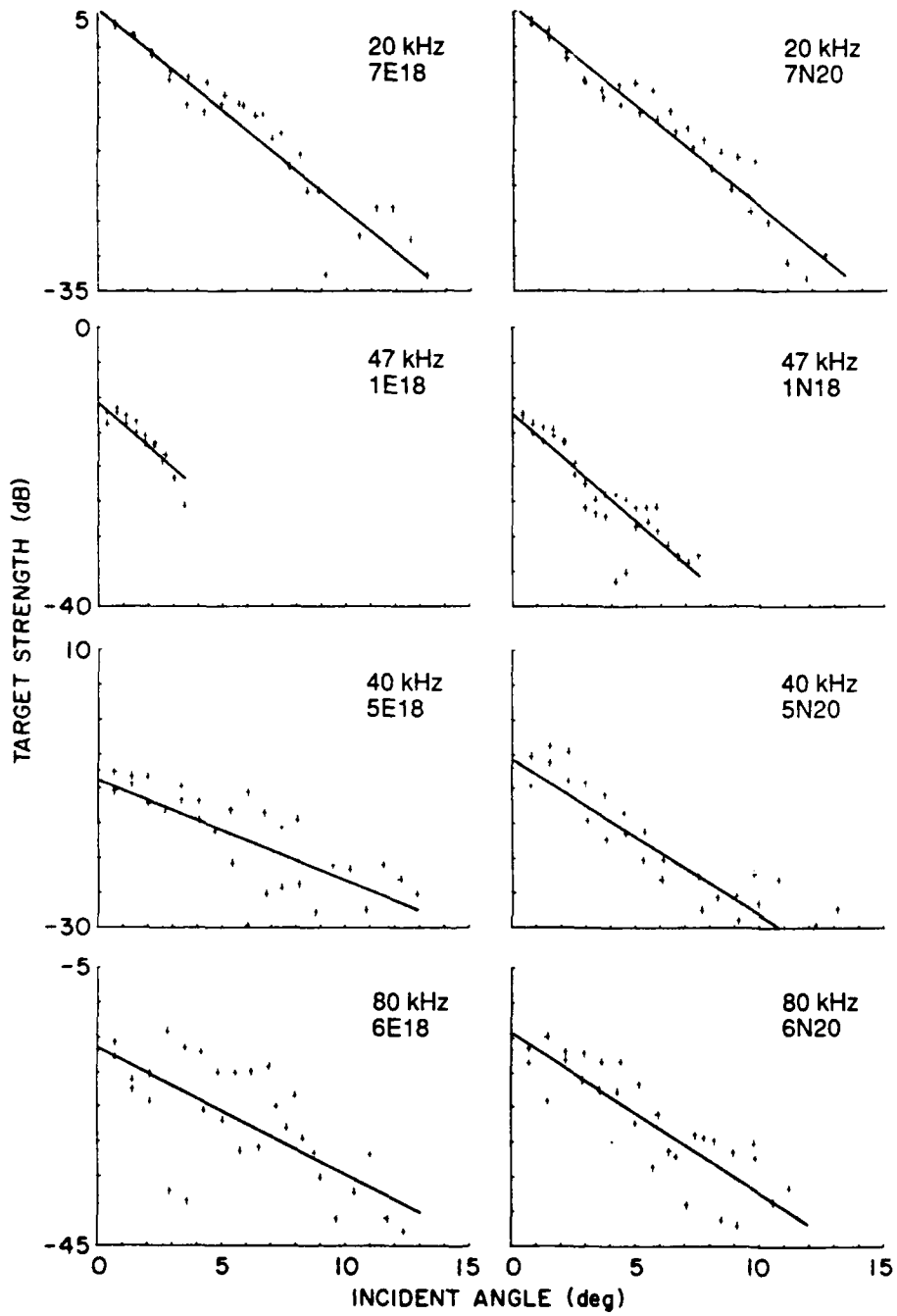


Figure 11c. A test of the empirical equation,  $TS = A - B\theta$ .

Table VII. Constants for the line  $TS = A - B\theta$ .

Frequency (kHz)	Run	A	Corrected <sup>b</sup>		Average Corrected		Average B
			A	A	A	B	
20	7N20	5.7	6.1			2.88	
	7E18	5.5	5.9			2.90	
	7E15	3.3	3.7	5.2	3.05		2.9
40	5N20	-5.7	-4.1			2.25	
	5E18	-8.8	-7.2	-5.7	1.44		1.9
47	1N18	-12.3	-11.9			3.10	
	1E18	-10.7	-10.3			3.15	
	2N16	-18.5	-18.1			3.29	
	2N18	-12.3	-11.9			4.23	
	2N19	-13.8	-13.4			3.66	
	2N20	-16.5	-16.1			3.16	
	2E16	-16.3	-15.9			4.05	
	2E17	-13.4	-13.0			4.41	
	2E18	-12.4	-12.0			4.43	
	2E20	-20.8	-20.4	-14.3	2.15		3.6
	80	3N19	-10.1	-8.8			2.41
3N20		-6.3	-5.0			2.90	
3N21		-7.2	-5.9			3.05	
3E15		-12.8	-11.5			2.69	
3E17		-11.5	-10.2			3.06	
3E18		-8.5	-7.2			2.64	
3E19		-8.5	-7.2	-8.1	3.10		2.8
6N20		-14.2	-6.5			2.31	
6N20 <sup>a</sup>		-13.7	-6.0			2.37	
6E18		-16.4	-8.7			1.83	
6E18 <sup>a</sup>		-17.4	-9.7	-7.7	1.94		2.1

<sup>a</sup>Using first echo only.<sup>b</sup>Corrected for near-field effect, using Table III.

The constant  $A$  is plotted against frequency in Fig. 12 and compared with the theoretical prediction based on the impedance change and rigid plate scattering. The discrepancy is fairly small at 20 kHz, but exceeds 20 dB at the higher frequencies. At these frequencies, it is also more or less constant. Such behavior would be expected if the effective roughness of the under surface was enough to cause phase changes in the return greater than  $2\pi$ , since this effect should reach a saturation point when the rms roughness  $\sigma$  is about  $\lambda/4$ . At 47 kHz, this saturation point would occur at  $\sigma = 0.8$  cm, which is in reasonable agreement with the size of the skeletal layer observed on the bottom of other blocks cut from the same area.

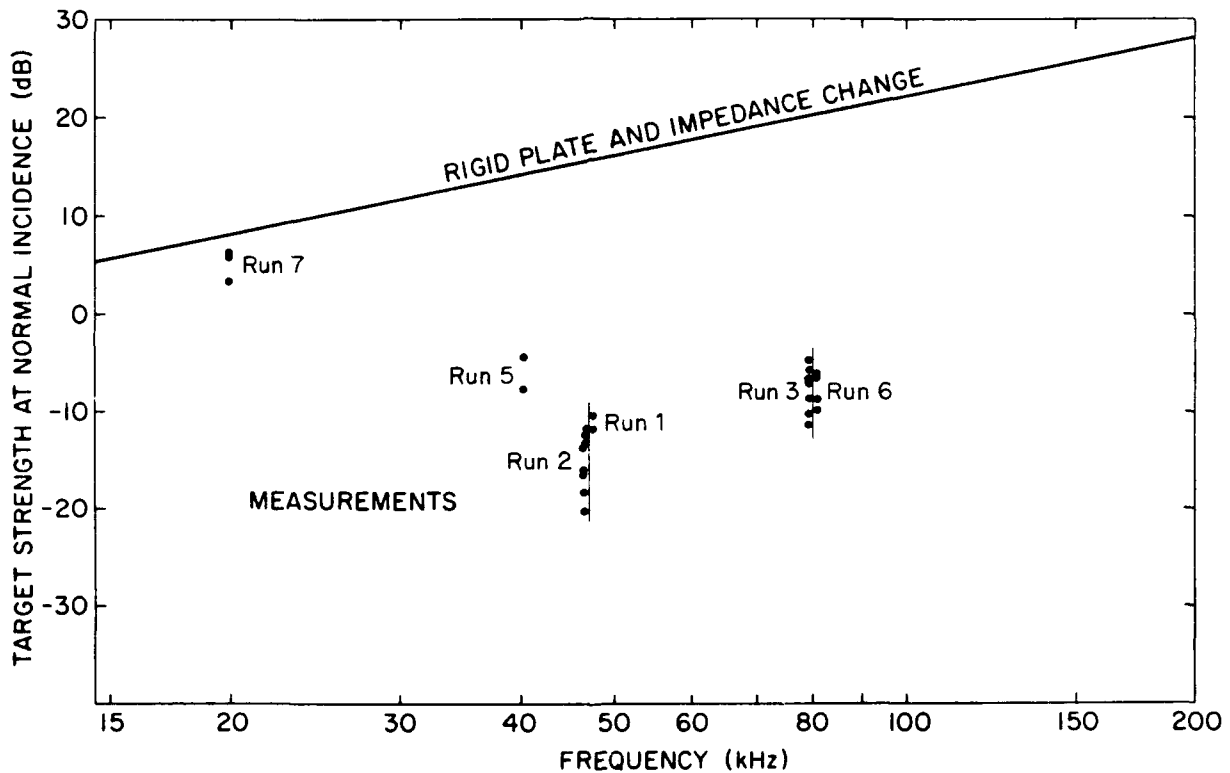


Figure 12. Measured target strengths at normal incidence, i.e., values of  $A$  in Table VII, corrected for near-field effects.

Although the dropoff in the return with increasing frequency, and the eventual saturation, appears to be an equivalent roughness effect, we do not have enough data to suggest an equation for the constant  $A$ . At 20 kHz the effect is small; at 40-80 kHz it may be 20-30 dB.

A plot of constant  $B$  versus frequency (Fig. 13) for the five sets of data shows considerable variation but no frequency dependence.

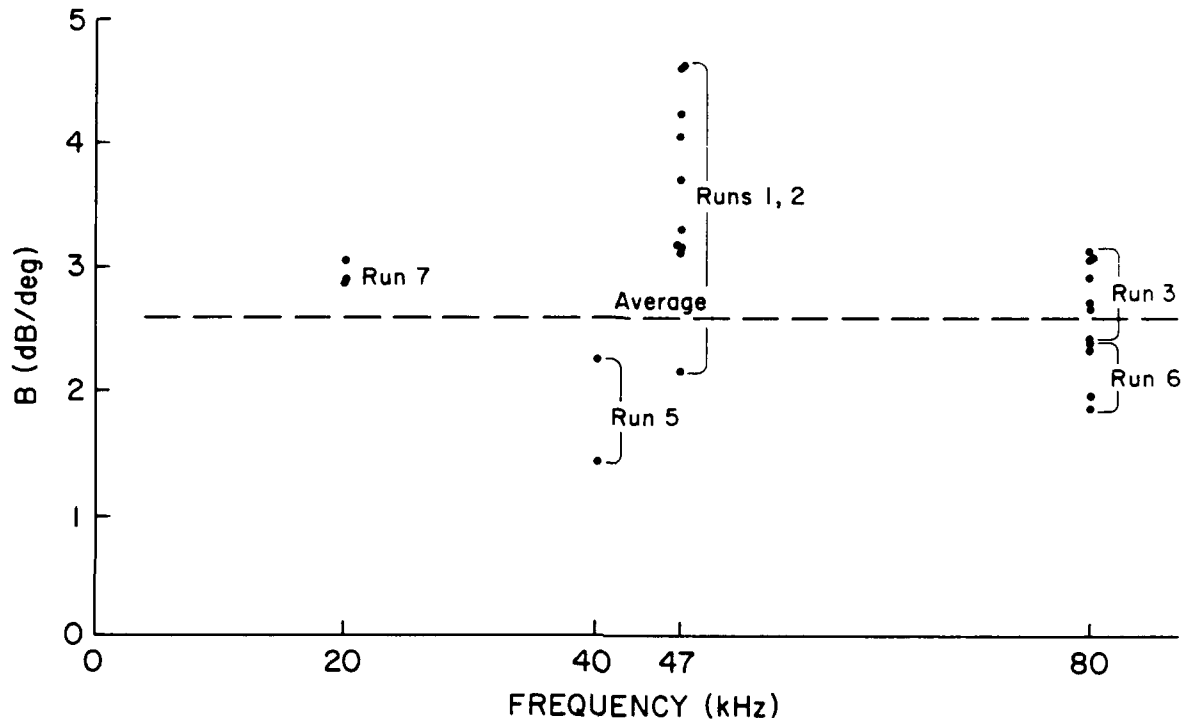


Figure 13. The constant  $B$  in Eq. 8 as determined from the measurements listed in Table VII.

## V. SUMMARY

The results of the 1984 ice block experiment can be summarized as follows:

1. The returns from an ice face at near normal incidence are smaller than the theoretical predictions calculated by combining the rigid plate pattern with the impedance change effect as in the Kirchhoff approximation. The difference varies from 3 dB at 20 kHz to as much as 30 dB at 47 kHz and above, and may be due to the inadequacy of the theory or to the structure at the ice-water boundary.

2. The acoustic response of the 0.84 m diam ice block dropped off about 10 dB at  $4^\circ$  from normal incidence for all frequencies (20-80 kHz). The -3 dB point occurred at a beam width of  $2.3^\circ$ . There was some variation in the beam width with frequency but no noticeable trend. Some sharp minima were observed in the acoustic response, but they did not agree with the side lobes predicted for a rigid plate.

3. The internal reflection from the submerged upper face of the block was observed at 80 kHz, indicating that the reflections from the back side of an ice block deserve further investigation.

## VI. DISCUSSION

In earlier work,<sup>1,8-11</sup> a detailed examination of some of the reflections from ice keels showed them to come from individual, separated reflectors with a narrow response pattern. A study of ice block configurations that would produce such reflections is necessary to understand ice-keel reflections.

The 1984 measurements reported here were made to examine a configuration that seems a likely source of such reflections, an ice block face at normal incidence. These may be the first measurements with an isolated ice block. Good control of the incident angle was important to the experiment. An examination of the bottom of the block by divers was desirable but prohibitive because of the possible contamination of the under surface with air bubbles. Additional measurements would have been prudent but the personnel and facilities were required for other projects.

The measurements indicate that this configuration could be a major source of ice keel reflections observed in the field, for the following reasons: (1) the measured target strength of the return (5 dB) and size of the block (0.84 m) correspond to those for a keel, (2) the response pattern was narrow, as observed in studies of returns from ice keels, (3) rough estimates indicate that there may be enough block faces present at near-normal incidence in a keel to produce a good portion of the observed reflectors.

By itself, the Kirchhoff approximation, which allows combining the effect of the impedance change on specular reflections of plane waves with the interference pattern for a rigid plate at a given incident angle, appears to be inadequate for predicting the return from in-situ ice surfaces at near-normal incidence. The effect of the porous ice structure at the lower boundary, which becomes more important at the shorter wavelengths, must be included. For the shorter wavelengths, this porous layer gives rise to a gradient in the characteristic impedance. At longer wavelengths, the effective impedance mismatch between ice and water will be more abrupt, and thus the interface is more reasonably modeled by considering the bulk properties of the two media.

The peak in the response pattern at normal incidence is a demonstration of Huygens' principle which gives the return in the far field as the sum of the in-phase contributions from all area increments of the surface. Any surface irregularity, if at an appreciable fraction of a wavelength, will greatly reduce this central peak, as was observed in the measurements.

The discovery that, at 80 kHz, the back side of the block contributes to the reflection means that further measurements must be made to investigate interior reflections and the absorption in the ice. The effect of the skeletal layer on the lower surface of the ice and of the submerged snow-covered surface above must also be investigated.

Some sharp minima were detected in the return at angles off normal incidence, but the spacing did not correspond to that predicted for an idealized flat, uniform surface. It would be helpful in the future to include a test on a block with the bottom layer cut off; the pattern of the return from a flat solid surface could then be measured in detail. This would eliminate the skeletal layer roughness and give a test of the use of the Kirchhoff approximation for an ice face.

Additional measurements are planned for 1986, using a block cut from thicker ice. After the first measurement, the block will be removed, the bottom layer cut off, and the block reset for another measurement. This will show the effect of the skeletal layer and give a measure of the absorption in the ice, if the upper surface is detectable. As a reference for calibration of the system we will also replace the ice block with a cylindrical block of air to give a flat surface with a high impedance change. Several diameters will be needed as a check on the area dependence of the theory. The acoustic measurements will be supplemented by detailed studies of the density, salinity, temperature, and void ratio of the ice, especially near the newly frozen surface. The lower surface will be characterized as to roughness during several stages of the freezing process.



## REFERENCES

1. G.R. Garrison, R.E. Francois, and T. Wen, "Acoustic return from ice keels, 1982 (U)," APL-UW 8311, Applied Physics Laboratory, University of Washington, Seattle, May 1984. (Confidential)
2. W.T. Ellison, "Simulation studies of under-ice acoustic scattering (U)," Cambridge Acoustical Associates, Inc., 54 Rindge Avenue Extension, Cambridge, Massachusetts, 15 October 1980. (Confidential)
3. C.S. Clay and H. Medwin, *Acoustical Oceanography: Principles and Applications* (John Wiley and Sons, New York), p. 507.
4. *Physics of Sound in the Sea* (Navmat P-9675, Department of the Navy, Headquarters, Naval Material Command, Washington, DC 20360, 1969).
5. G.R. Garrison, T. Wen, and M.L. Welch, "Environmental measurements in the Beaufort Sea, Autumn 1984," APL-UW 3-85, Applied Physics Laboratory, University of Washington, Seattle, March 1985.
6. D.F. McCammon and S.T. McDaniel, "The influence of the physical properties of ice on reflectivity," *J. Acoust. Soc. Am.* 77:499-507 (1985).
7. R.J. Urick, *Principles of Underwater Sound* (McGraw-Hill, New York, 1975).
8. G.R. Garrison, R.E. Francois, E.W. Early, and T. Wen, "Comprehensive studies of arctic pack ice in April 1976," APL-UW 7724, Applied Physics Laboratory, University of Washington, Seattle, May 1978.
9. R.E. Francois, G.R. Garrison, E.W. Early, T. Wen, and J.T. Shaw, "Acoustic measurements under shore-fast ice in summer 1977 (U)," APL-UW 7825, Applied Physics Laboratory, University of Washington, Seattle, March 1981. (Confidential)
10. R.E. Francois and G.R. Garrison, "Under-ice topography as detailed by a narrow-beam sonar (U)," *U.S. Navy J. Underwater Acoustics* 30:299-422 (1980). (Confidential)
11. G.R. Garrison, R.E. Francois, and T. Wen, "Ice keels as false targets (U)," *U.S. Navy J. Underwater Acoustics* 30:423-437 (1980). (Confidential)

Distribution List

Assistant Secretary of the Navy  
(Research, Engineering and Systems)  
Department of the Navy  
Washington, DC 20350 [2 cp]

Chief of Naval Operations  
Department of the Navy  
Washington, DC 20350

OP02 (COMO R. Zeller)  
OP006 (RADM C. Schultz)  
OP006T (R.S. Winokur)  
OP095 (VADM J.R. Hogg)  
OP098 (VADM A.J. Baciocco, Jr.)  
OP22 (COMO J. Reynolds)  
OP226  
OP951 (R. Pittenger)

Director of Defense Research and Engineering  
Office of Assistant Director (Ocean Control)  
The Pentagon  
Washington, DC 20301

Chief of Naval Research  
Department of the Navy  
800 North Quincy Street  
Arlington, VA 22217

OCNR00 (RADM J. Mooney, Jr.)  
OCNR112 (G. Hamilton)  
OCNR 1125 (R. Obrachta) [2 cp]  
OCNR 922 (R.A. Nagelhout)

Office of Naval Research<sup>c</sup>  
R. Silverman, Resident Representative  
315 University District Bldg., JD-16  
1107 N.E. 45th Street  
Seattle, WA 98195

Office of Naval Research Field Detachment  
Code 920  
Bay St. Louis  
NSTL Station, MS 39529-5000  
Code 920 (R. Gardner)

Office of Naval Technology  
Department of the Navy  
Ballston Center Tower #1  
800 N. Quincy Street  
Arlington, VA 22217  
OCNR 22 (G. Spalding)  
OCNR 23 (A.J. Faulstich)  
OCNR 232 Undersea Warfare Weaponry  
OCNR 234 (T. Warfield)

Commander  
Naval Air Systems Command Hq.  
Department of the Navy  
Washington, DC 20361 [2 cp]

Commander  
Naval Space and Warfare Systems Command (NC1)  
(SPAWAR)  
Department of the Navy  
Washington, DC 20363-5100  
SPAWAR 03 (Deputy CMDR J.H. Mills, Jr.)

Commander  
Arctic Submarine Laboratory  
Naval Ocean Systems Center  
Bldg. 371  
San Diego, CA 92132  
Code 19 (CAPT M. Dorman)

Commander  
Naval Sea Systems Command  
Department of the Navy  
Washington, DC 20362

NSEA 06<sup>c</sup> (RADM Ming Chang)  
NSEA 06U (J. Grembi)  
NSEA 06UR (R. Smith)  
Code 06B<sup>c</sup> [3 cp]  
NSEA 063R<sup>c</sup> (C.D. Smith) [2 cp]  
NSEA 63RB1 (A. Franceschetti)  
NSEA 63R2 (H. Magid)  
NSEA 63R3 (F. Romano)  
NSEA 63Z (CAPT J. Carlson)  
Code 99612<sup>c</sup> [4 cp]  
Code PMS-402 (CAPT P. Chabot)  
Code PMS-402 (D. Houser)  
Code PMS-407 (CAPT L.E. Wood)  
Code PMS-407 (D. Porter)  
Code PMS-4074 (J. Singletary)

Commander  
Naval Weapons Center  
China Lake, CA 93555  
Library

Commander  
Naval Ocean Systems Center  
San Diego, CA 92152  
Library [4 cp]  
Code 19 [2 cp]  
Code 6352 (R.J. Vent)  
Code 654 (F. Legerman)  
Code 65 (W. Brandon)

Commander  
Naval Air Development Center  
Warminster, PA 18974

Commander  
David W. Taylor Naval Ship Research  
and Development Center  
Bethesda, MD 20084

Commander  
Naval Surface Weapons Center  
White Oak  
Silver Spring, MD 20910  
Code U42 (M.M. Klinerman)  
Library [2 cp]  
Code U06 [2 cp]

Commander, SECOND Fleet  
Fleet Post Office  
New York, NY 09501

Commander, THIRD Fleet  
Fleet Post Office  
San Francisco, CA 96601

Commander Submarine Force  
U.S. Atlantic Fleet  
Norfolk, VA 23511

Commander Submarine Force  
U.S. Pacific Fleet  
N-21  
FPO San Francisco, CA 96601

Commander  
Submarine Squadron THREE  
Fleet Station Post Office  
San Diego, CA 92132

Commander  
Submarine Group FIVE  
Fleet Station Post Office  
San Diego, CA 92132

Commander  
Submarine Development Squadron TWELVE  
Box 70  
Naval Submarine Base - New London  
Groton, CT 06340

Director  
Defense Advanced Research Project Agency  
1400 Wilson Boulevard  
Arlington, VA 22209

Commanding Officer  
Naval Intelligence Support Center  
4301 Suitland Road  
Washington, DC 20390

Commanding Officer  
Naval Coastal Systems Center  
Panama City, FL 32407

Commanding Officer  
Naval Underwater Systems Center  
Newport, RI 02840

Library [5 cp]  
Code 01Y (E. Simmons)  
Code 8321 (J.R. Short)  
Code 8212 (C. Albanese)  
Code 801 (F. Aidala, Jr.)  
Code 6291 (A.S. Davis)  
Code 81 (P. Labrecque)

Officer-in-Charge  
New London Laboratory  
Naval Underwater Systems Center  
New London, CT 06320 [2 cp]

Library  
Code 3302 [2 cp]

Commanding Officer  
Naval Ocean Research and Development Activity  
NSTL Station, MS 39529

Code 113 (B. Adams) [2 cp]  
Code 243 (R. Farwell)  
Code 200 (W.B. Moseley)  
Code 240 (J. Ford)  
Code 242 (D. Ramsdale) [2 cp]  
Code 270 (W.A. Kuperman)  
Code 332 (J. Welsh, Jr.)

Commanding Officer  
Naval Submarine School  
Box 70  
Naval Submarine Base - New London  
Groton, CT 06340

Superintendent  
U.S. Navy Postgraduate School  
Monterey, CA 93940

Library [2 cp]

Office of the Director  
Naval Oceanography Division  
Navy Department  
Washington, DC 20350 [2 cp]  
Code OP-006D (CAPT C. Hoffman)

Director  
Applied Physics Laboratory  
University of Washington  
1013 N.E. 40th Street  
Seattle, WA 98105

C.G. Sienkiewicz  
R.E. Francois  
G.R. Garrison  
D.R. Jackson  
E.I. Thorsos  
J.G. Dworski  
R.P. Stein  
T. Wen  
D.P. Winebrenner  
Library

Polar Research Laboratory, Inc.  
6309 Carpenteria Avenue  
Carpenteria, CA 90813

Honeywell  
Marine Systems Division  
5303 Shulshole Avenue N.W.  
Seattle, WA 98107

Mayer Freedman

Hughes Aircraft  
1901 W. Malvern Road  
P.O. Box 3310  
Fullerton, CA 92634

P. Norman

Commanding Officer  
Naval Oceanographic Office  
Bay St. Louis  
NSTL Station, MS 39522

Code 7300 (W. Jobst)  
Code 7320 (R. Christensen)

Director  
Naval Research Laboratory  
Washington, DC 20375

Technical Information Division [3 cp]  
Acoustics Division (D. Bradley)

Director  
Applied Research Laboratory  
Pennsylvania State University  
State College, PA 16801

C. Ackerman  
R. Ingram [2 cp]  
S. McDaniel  
F. Symons, Jr.

Director  
Applied Research Laboratories  
The University of Texas at Austin  
P.O. Box 8029  
Austin, TX 78713-8029 [2 cp]

REPORT DOCUMENTATION PAGE		READ INSTRUCTIONS BEFORE COMPLETING FORM
1. REPORT NUMBER APL-UW 8506	2. GOVT ACCESSION NO.	3. RECIPIENT'S CATALOG NUMBER
4. TITLE (and Subtitle) MEASUREMENTS OF ACOUSTIC REFLECTION FROM THE END OF A CYLINDRICAL BLOCK OF ARCTIC ICE		5. TYPE OF REPORT & PERIOD COVERED
		6. PERFORMING ORG. REPORT NUMBER APL-UW 8506
7. AUTHOR(s) G.R. Garrison, R.E. Francois, T. Wen, and R.P. Stein		8. CONTRACT OR GRANT NUMBER(s) N00024-81-C-6042 N00024-85-C-6264
9. PERFORMING ORGANIZATION NAME AND ADDRESS Applied Physics Laboratory University of Washington 1013 N.E. 40th Street Seattle, WA 98105		10. PROGRAM ELEMENT PROJECT, TASK AREA & WORK UNIT NUMBERS PE62759N
11. CONTROLLING OFFICE NAME AND ADDRESS Naval Sea Systems Command (Code 63R) Department of the Navy Washington, DC 20362		12. REPORT DATE September 1986
		13. NUMBER OF PAGES 42
14. MONITORING AGENCY NAME & ADDRESS (if different from Controlling Office) Naval Ocean Research & Development Activity, Code 245 NSTL Station, MS 39522		15. SECURITY CLASS. (of this report) UNCLASSIFIED
		15a. DECLASSIFICATION/DOWNGRADING SCHEDULE
16. DISTRIBUTION STATEMENT (of this Report)  Distribution unlimited; approved for public release.		
17. DISTRIBUTION STATEMENT (of the abstract entered in Block 20, if different from Report)		
18. SUPPLEMENTARY NOTES		
19. KEY WORDS (Continue on reverse side if necessary and identify by block number) Acoustic reflection from ice, Ice block target strength, Target strength of ice.		
20. ABSTRACT (Continue on reverse side if necessary and identify by block number) In the fall of 1984 an experiment was conducted at an arctic ice camp to examine 20-80 kHz acoustic reflections from an isolated ice block. The results are compared with a simple model of ice block reflections that has been used in conjunction with an ice block configuration for pressure ridge keels. The study of the reflections from these keels is important because they form an interfering background for acoustic equipment operating under the ice. A cylindrical block of ice 0.84 m in diameter was cut from the flat surface of a floe and depressed so that, for a transducer placed below, the reflection from		

ABSTRACT, Cont'd.

the block would arrive before that from the surrounding ice. A transducer 15-30 m below the block was moved horizontally in steps to measure changes with aspect. The returns from the block are compared with those predicted by the model, which includes a loss based on the bulk impedance properties of the two media. When near field effects are included, the measured returns at 20 kHz are similar to those predicted; but as the frequency is increased, the return at normal incidence is lower than predicted and the response pattern is broadened and smoothed. The complex structure of the growing sea ice, producing both volume and surface acoustic scattering, is the most likely cause of the discrepancy.